Received: 30 September 2019 | Accepted: 10 December 2019
DOI: 10.1002/adc2.29

SPECIAL ISSUE ARTICLE

WILEY

Controllability analysis and controller design for variable-pitch propeller quadcopters with one propeller failure

Zhikun Wang[1] | **Roderich Groß**[1] | **Shiyu Zhao**[2,3]

[1]Department of Automatic Control and Systems Engineering, The University of Sheffield

[2]School of Engineering, Westlake University

[3]Institute of Advanced Technology, Westlake Institute for Advanced Study

Correspondence
Shiyu Zhao, School of Engineering, Westlake University, Hangzhou, China.
Email: zhaoshiyu@westlake.edu.cn

This article studies a relatively new type of aerial platform: variable-pitch propeller (VPP) quadcopters. Unlike conventional fixed-pitch propellers that can only generate upward thrust forces, a VPP can adjust its pitch angle to generate either upward or downward thrust forces. This provides VPP quadcopter with high agility and strong maneuverability. Although VPP quadcopters have attracted some attention recently, their potential has not been fully explored yet. In this article, we study the fault-tolerant property of VPP quadcopters when one of the four VPPs fails to provide any forces or torques. We identify the equilibrium state in this case and conduct the controllability analysis based on a linearized model. This shows that the system remains controllable even if one propeller fails. As a result, simple linear-quadratic regulator controllers can be used to control the platform. Although the controllability analysis and controller are based on the linearized model, numerical simulation incorporating measurement noises and external disturbances verifies the theoretic findings.

KEYWORDS
controllability analysis, fault-tolerant control, quadcopters, variable pitch propeller

1 | INTRODUCTION

Quadcopter unmanned aerial vehicles have become a popular platform for many aerial applications such as aerial photography, surveillance, and transportation. Compared with other applications, safety-critical tasks such as parcel delivery and passenger transportation pose higher requirements about the safety and reliability of the platform. To improve the safety and reliability of the quadcopter platform, there are many methods.[1] One of them is to apply the fault-tolerant control method, which allows the quadcopter to maintain a relatively stable state in the presence of one or more faults such as motor failures.[2,3] This method has attracted extensive studies due to its great importance.[4-7]

In this article, we study a specific yet important type of aerial platforms: variable-pitch propeller (VPP) quadcopters. This type of platform is similar to conventional quadcopter platforms in terms both mechanical and control structures. The key difference is that a VPP can adjust its pitch angle and hence generate both upward and downward thrusts. Although the mechanics of VPPs are more complicated than conventional propellers, the overall mechanical structure and the control system structure of VPP quadcopters are the same as the conventional ones.

A slight mechanical complexity increase of the VPPs brings many interesting and attractive features. First, regarding the direction of propeller thrust forces, each VPP can generate both upward and downward thrust forces, whereas a fixed-pitch propeller of a conventional quadcopter can only generate upward thrust forces. This provides VPP quadcopters with strong maneuverability. For example, a VPP quadcopter can hover upside down, which is not feasible for conventional quadcopters. Second, regarding the control bandwidth, the magnitude of the thrust force generated by a VPP can be adjusted efficiently by controlling the propeller pitch angle through the associated actuator of the VPP. As a comparison, a conventional quadcopter can only adjust the force magnitude of a propeller by speed control. The response of speed control is much slower than actuator control.[8,9] This brings high agility to VPP quadcopters. Due to these features, VPP quadcopters have attracted some attention recently.[10-12] However, their potential has not been fully explored yet.

In this article, we explore a new fault-tolerant feature of VPP quadcopters. For conventional quadcopters, when one or more motors/propellers fail to work properly, the platforms usually become extremely hard to control and sophisticated controllers must be designed.[13,14] More importantly, even under fault-tolerant controllers, conventional quadcopters with faults are only able to fly in very special manners such as continuously rotating.[15-17] By contrast, VPP quadcopters shows strong fault-tolerant ability as we show in this article.

The contributions of this article are as follows. First, we conduct the controllability analysis of a VPP quadcopter with one propeller failure based on the linearized dynamical model. It is shown that, when one propeller fails, all states of the quadcopter remain controllable. For comparison purposes, we also analyze the controllability of fixed-pitch quadcopters with one motor failure and show that fixed-pitch quadcopters are uncontrollable with motor failures. Second, we identify the equilibrium point and derive the linearized dynamical model of VPP quadcopters. Based on the linearized model, we design an linear-quadratic regulator (LQR) controller to handle propeller failure. Using this simple controller, the VPP quadcopter can accurately track a given trajectory even if subjected to wind disturbances or noise. This property is important for safety-critical tasks such as flying taxi, where it is necessary to transport the human passengers to a safe place securely in the presence of propeller failures. Thanks for this property, VPP quadcopters provide an important alternative platform for safety-critical aerial tasks.

It is worth mentioning that we do not consider fault detection, isolation, or switching controllers in this article. These important topics will be addressed in our future work. The focus of this article is to explore the fault-tolerant ability of VPP quadcopters, which has not been reported in the literature.

This article is organized as follows. Section 2 presents the dynamical model of VPP quadcopters in the presence of one propeller failure. Section 3 presents the linearized model and analyzes the system controllability. Section 4 shows comprehensive simulation results. Conclusions are drawn in Section 5.

2 | DYNAMIC MODEL OF VPP QUADCOPTERS

The mechanical structure of a VPP quadcopter is shown in Figure 1. It is notable that its overall structure is the same as a conventional fixed-pitch quadcopter. The state vector is $\mathbf{x} = [x, y, z, \phi, \theta, \psi, p, q, r, u, v, w]^T \in \mathbb{R}^{12}$, where (x, y, z), (ϕ, θ, ψ), (p, q, r), and (u, v, w) denote the position, attitude, angular velocity, and linear velocity, respectively. The rotation from the body frame to the global frame is described by the rotational matrix $\mathbf{R} \in SE(3)$.

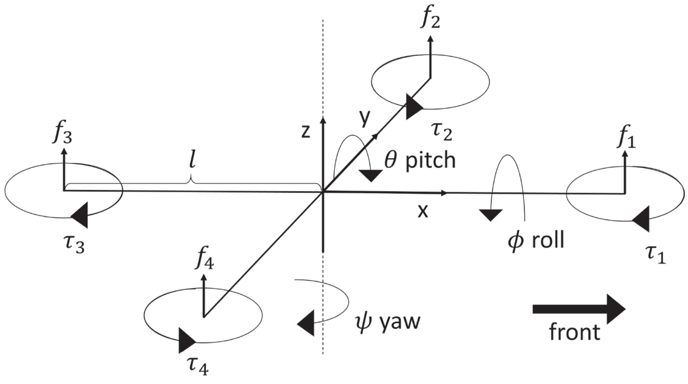

FIGURE 1 The mechanical structure of a variable-pitch propeller quadcopter

Let f_1,f_2,f_3,f_4 be the forces generated by propellers 1 to 4, where propellers 1 and 3 spin clockwise and propellers 2 and 4 spin counterclockwise, and $\tau_1, \tau_2, \tau_3, \tau_4$ be the torques generated by propellers 1 to 4, respectively.

The dynamics of the VPP quadcopter are described by

$$\dot{\mathbf{x}} = \begin{bmatrix} \dot{x} \\ \dot{y} \\ \dot{z} \\ \dot{\phi} \\ \dot{\theta} \\ \dot{\psi} \\ \dot{p} \\ \dot{q} \\ \dot{r} \\ \dot{u} \\ \dot{v} \\ \dot{w} \end{bmatrix} = \begin{bmatrix} u \\ v \\ w \\ p + q\sin\phi\tan\theta + r\cos\phi\tan\theta \\ q\cos\phi - r\sin\phi \\ q\sin\phi\sec\theta + r\cos\phi\sec\theta \\ qr\frac{I_z - I_y}{I_x} + u_2\frac{l}{I_x} \\ rp\frac{I_x - I_z}{I_y} + u_3\frac{l}{I_y} \\ pq\frac{I_y - I_x}{I_z} + u_4\frac{l}{I_z} \\ \frac{(\cos\psi\sin\theta\cos\phi + \sin\psi\sin\phi)u_1 - d_x u}{m} \\ \frac{(\sin\psi\sin\theta\cos\phi - \cos\psi\sin\phi)u_1 - d_y v}{m} \\ (\cos\theta\cos\phi)u_1/m - d_z w/m - g \end{bmatrix}, \tag{1}$$

where l is the length of each quadcopter arm, m is the mass of the quadcopter, g denotes the gravitational constant, and I_x, I_y, I_z are the moment of inertia. In our work, suppose $m = 1$ kg, $g = 10m^2/s$, and $l = 0.35$ m.

The control inputs, $\mathbf{u} = [u_1, u_2, u_3, u_4]^T \in \mathbb{R}^4$, are

$$\mathbf{u} = \begin{bmatrix} u_1 \\ u_2 \\ u_3 \\ u_4 \end{bmatrix} = \begin{bmatrix} f_1 + f_2 + f_3 + f_4 \\ f_3 - f_1 \\ f_4 - f_2 \\ \tau_1 - \tau_2 + \tau_3 - \tau_4 \end{bmatrix}. \tag{2}$$

The pitch angle of VPP propeller i is denoted as α_i, which could be positive or negative. The spinning speed of motor i is ω_i, which is positive. The force and torque generated by VPP propeller i are

$$f_i = k_1\omega_i^2\alpha_i, \tag{3}$$

$$\tau_i = k_2\omega_i^2 + k_3\omega_i^2\alpha_i^2 + k_4\omega_i\alpha_i,$$

where k_1, k_2, k_3, k_4 are constant parameters determined by the motor and air resistance.[18,19] In our work, suppose $k_1 = 5 \times 10^{-7}$, $k_2 = 1 \times 10^{-8}$, $k_3 = 2 \times 10^{-10}$, and $k_4 = 4 \times 10^{-7}$. Note that the torque generated by a VPP can be nonzero even when the pitch angle and its force are zero.

There are two types of power supply modes for VPP quadcopters. One is the centralized power mode, where the spin of all propellers is powered by a central motor placed at the center of the quadcopter. In this case, all the propellers have the same and fixed spinning speed.[20] The other is the decentralized power mode, where the spin of each propeller is powered by an independent motor. In this case, the spinning speeds of different propellers may be different.[9] In this article, we consider the decentralized power mode, where both α_i and ω_i can be adjusted independently by each propeller. In this work, suppose that the maximum spinning speed of each independent motor is 10 000 rpm, and the pitch angle of each propeller varies in the interval of $[-15, 15]$ deg ($[-0.26, 0.26]$ rad). Substituting Equation (3) into Equation (2) gives

$$
\begin{aligned}
u_1 &= k_1(\omega_1^2\alpha_1 + \omega_2^2\alpha_2 + \omega_3^2\alpha_3 + \omega_4^2\alpha_4),\\
u_2 &= k_1(\omega_3^2\alpha_3 - \omega_1^2\alpha_1),\\
u_3 &= k_1(\omega_4^2\alpha_4 - \omega_2^2\alpha_2),\\
u_4 &= k_2(\omega_3^2 + \omega_1^2 - \omega_2^2 - \omega_4^2)\\
&\quad + k_3(\omega_3^2\alpha_3^2 + \omega_1^2\alpha_1^2 - \omega_2^2\alpha_2^2 - \omega_4^2\alpha_4^2)\\
&\quad + k_4(\omega_3\alpha_3 + \omega_1\alpha_1 - \omega_2\alpha_2 - \omega_4\alpha_4).
\end{aligned}
$$

When there is a propeller failure, $\mathbf{u}$ would be different. Without loss of generality, suppose propeller 1 fails such that it provides zero force and zero torque. That is, f_1 and τ_1 are always zero. Then, $\mathbf{u}$ becomes

$$
\begin{aligned}
u_1 &= k_1(\omega_2^2\alpha_2 + \omega_3^2\alpha_3 + \omega_4^2\alpha_4),\\
u_2 &= k_1\omega_3^2\alpha_3,\\
u_3 &= k_1(\omega_4^2\alpha_4 - \omega_2^2\alpha_2),\\
u_4 &= k_2(\omega_3^2 - \omega_2^2 - \omega_4^2)\\
&\quad + k_3(\omega_3^2\alpha_3^2 - \omega_2^2\alpha_2^2 - \omega_4^2\alpha_4^2)\\
&\quad + k_4(\omega_3\alpha_3 - \omega_2\alpha_2 - \omega_4\alpha_4).
\end{aligned} \tag{4}
$$

Although propeller 1 fails, there remain six independent control quantities, $\omega_2, \omega_3, \omega_4$ and $\alpha_2, \alpha_3, \alpha_4$. To generate desired $\mathbf{u}$, the six control quantities are still redundant, which is the fundamental reason why the system remains controllable in the presence of a propeller failure.

3 | LINEARIZATION AND CONTROLLABILITY ANALYSIS

In this section, we identify the equilibrium point of the system in the presence of a propeller failure, linearize the system at the equilibrium point, and conduct controllability analysis. To limit the risk of excessive vibration or propeller stall,[8] we assume that all ω_i are bounded by $[0, 10\,000]$ rpm and all α_i are bounded by $[-0.26, 0.26]$ rad.

3.1 | Equilibrium point

Consider a desired state

$$\mathbf{x}^* = \left[x^*, y^*, z^*, 0, 0, \psi^*, 0, 0, 0, 0, 0, 0\right]^T.$$

In order to keep the system at this state, the input must be

$$\mathbf{u}^* = [mg, 0, 0, 0]^T. \tag{5}$$

Substituting Equation (5) into Equation (4) yields

$$mg = k_1\omega_2^2\alpha_2 + k_1\omega_3^2\alpha_3 + k_1\omega_4^2\alpha_4, \tag{6}$$

$$0 = k_1\omega_3^2\alpha_3, \tag{7}$$

$$0 = k_1\omega_4^2\alpha_4 - k_1\omega_2^2\alpha_2, \tag{8}$$

$$
\begin{aligned}
0 &= k_2(\omega_3^2 - \omega_2^2 - \omega_4^2)\\
&\quad + k_3(\omega_3^2\alpha_3^2 - \omega_2^2\alpha_2^2 - \omega_4^2\alpha_4^2)\\
&\quad + k_4(\omega_3\alpha_3 - \omega_2\alpha_2 - \omega_4\alpha_4).
\end{aligned} \tag{9}
$$

The next step is to solve the above equations. Equation (7) implies that $\omega_3^2\alpha_3 = 0$. It is implied from Equation (9) that $\omega_3 \neq 0$; otherwise, the right-hand side of Equation (9) is less than zero. As a result, we know $\alpha_3 = 0$ and $\omega_3 \neq 0$, which means that propeller 3 still spins but with zero pitch angle. On the other hand, Equations (6), (7), and (8) imply

$$k_1\omega_2^2\alpha_2 = k_1\omega_4^2\alpha_4 = \frac{mg}{2}, \tag{10}$$

which means that propellers 2 and 4 provide forces to counter gravity. Without loss of generality, suppose

$$\omega_2 = \omega_4. \tag{11}$$

As a result,

$$\alpha_2 = \alpha_4, \tag{12}$$

Substituting Equations (11) and (12) into Equation (9) gives

$$k_2\omega_3^2 = 2(k_2\omega_2^2 + k_3\omega_2^2\alpha_2^2 + k_4\omega_2\alpha_2). \tag{13}$$

Substituting Equation (10) into Equation (13) yields

$$k_2\omega_3^2 = 2\left[k_2\omega_2^2 + \frac{k_3}{k_1^2}\left(\frac{mg}{2\omega_2}\right)^2 + \frac{k_4mg}{2k_1\omega_2}\right] := r(\omega_2), \tag{14}$$

where $r(\omega_2)$ represents the right-hand side of Equation (14).

Next we identify the range of the value of $r(\omega_2)$. The derivative of $r(\omega_2)$ with respect to ω_2 is

$$\frac{\mathrm{d}r(\omega_2)}{\mathrm{d}\omega_2} = 2\left(2k_2\omega_2 - \frac{k_3m^2g^2}{2k_1^2\omega_2^3} - \frac{k_4mg}{2k_1\omega_2^2}\right). \tag{15}$$

By analyzing Equation (15), we notice that $r(\omega_2)$ is a monotonically increasing function when $\omega_2 \in [0, 10\,000]$. In addition, Equation (10) implies that, when the pitch angle takes the maximum value $\alpha_2 = 0.26$, the rotating speed would take the minimum value $\omega_2 = 6201$. As a result, $\omega_2 \in [6201, 10\,000]$. Substituting the interval into Equation (14) gives $r(\omega_2) \in [0.7714, 2]$. Meanwhile, the left-hand side of Equation (14) satisfies $k_2\omega_3^2 \in [0, 1]$ when $\omega_3 \in [0, 10\,000]$. By combining the bounds of the left- and right-hand sides of Equation (14), we know

$$k_2\omega_3^2 = r(\omega_2) \in [0.7714, 1]. \tag{16}$$

Substituting Equation (16) into Equation (14) yields $\omega_2 \in [6201, 7067]$ and $\omega_3 \in [8782, 10\,000]$. We simply choose $\omega_3 = 9000$, an intermediate value in $[8782, 10\,000]$. Note that ω_3 remains constant all the time.

By substituting $\omega_3 = 9000$ into Equation (14), we can obtain four solutions: $\omega_2^* = -217$, 227, 6355, and -6365. As $\omega_2 \in [6201, 7067]$ as aforementioned, $\omega_2^* = 6355$ is the only feasible solution. Then, substituting ω_2^* into Equation (10) gives $\alpha_2^* = 0.2476$.

Let $\mathbf{z} = [\omega_2, \alpha_2, \alpha_3, \alpha_4]^T$. It follows from the above analysis that, in order to keep the system at the state $\mathbf{x}^*$, $\mathbf{z}$ should be

$$\begin{aligned}\mathbf{z}^* &= \left[\omega_2^*, \alpha_2^*, \alpha_3^*, \alpha_4^*\right]^T \\ &= \left[6355, 0.2476, 0, 0.2476\right]^T.\end{aligned}$$

3.2 | Linearized model

To linearize the nonlinear dynamical system, consider $\overline{\mathbf{z}} = \mathbf{z} - \mathbf{z}^*$ and $\overline{\mathbf{x}} = \mathbf{x} - \mathbf{x}^*$. Let $\mathbf{F}(\overline{\mathbf{x}}, \overline{\mathbf{z}}) \in \mathbb{R}^{12}$ be the right-hand side of Equation (1). Then, the linearized model is

$$\dot{\overline{\mathbf{x}}} = \mathbf{A}\overline{\mathbf{x}} + \mathbf{B}\overline{\mathbf{z}},$$

where

$$\mathbf{A} = \left.\frac{\partial \mathbf{F}(\overline{\mathbf{x}}, \overline{\mathbf{z}})}{\partial \mathbf{x}}\right|_{\mathbf{x}=\mathbf{x}^*,\mathbf{z}=\mathbf{z}^*}$$

$$= \begin{bmatrix} 0_{3\times3} & 0_{3\times3} & 0_{3\times3} & \mathbf{I}_{3\times3} \\ 0_{3\times3} & 0_{3\times3} & \mathbf{I}_{3\times3} & 0_{3\times3} \\ 0_{3\times3} & 0_{3\times3} & 0_{3\times3} & 0_{3\times3} \\ 0_{3\times3} & \mathbf{E}_{3\times3} & 0_{3\times3} & 0_{3\times3} \end{bmatrix} \in \mathbb{R}^{12\times12},$$

$$\mathbf{E}_{3\times3} = \begin{bmatrix} g\sin\psi^* & g\cos\psi^* & 0 \\ -g\cos\psi^* & g\sin\psi^* & 0 \\ 0 & 0 & 0 \end{bmatrix},$$

and

$$\mathbf{B} = \left.\frac{\partial \mathbf{F}(\overline{\mathbf{x}}, \overline{\mathbf{z}})}{\partial \mathbf{z}}\right|_{\mathbf{x}=\mathbf{x}^*,\mathbf{z}=\mathbf{z}^*}$$

$$= \begin{bmatrix} 0 & 0 & 0 & 0 \\ 0 & 0 & 0 & 0 \\ 0 & 0 & 0 & 0 \\ 0 & 0 & 0 & 0 \\ 0 & 0 & 0 & 0 \\ 0 & 0 & 0 & 0 \\ 0 & h_3\frac{l}{I_x} & 0 & 0 \\ -h_2\frac{l}{I_y} & 0 & -h_4\frac{l}{I_y} & n_4 - n_2 \\ -m_2 & m_3 & -m_4 & -o_2 - o_4 \\ 0 & 0 & 0 & 0 \\ 0 & 0 & 0 & 0 \\ \frac{k_1}{m}\omega_2^{*2} & \frac{k_1}{m}\omega_3^{*2} & \frac{k_1}{m}\omega_4^{*2} & p_4 + p_2 \end{bmatrix} \in \mathbb{R}^{12\times4},$$

with

$$h_i = k_1\omega_i^{*2},$$
$$m_i = 2k_3\alpha_i^*\omega_i^{*2} + k_4\omega_i^*,$$
$$n_i = 2k_1\omega_i^*\alpha_i^*\frac{l}{I_y},$$
$$o_i = (2k_2\omega_i^* + 2k_3\omega_i^*\alpha_i^{*2} + k_4\alpha_i^*)\frac{l}{I_z},$$
$$p_i = 2\frac{k_1}{m}\omega_i^*\alpha_i^*.$$

3.3 | Controllability analysis of VPP quadcopters

It can be calculated that the rank of the controllability matrix is rank($\mathbf{Q}$) = rank[$\mathbf{BABA}^2\mathbf{B} \dots \mathbf{A}^{11}\mathbf{B}$] = 12. As a result, the controllability matrix is of full row rank. Hence, all the states remain controllable when one propeller fails. Although the controllability is analyzed based on the linearized system, we show later by simulation that the nonlinear model of a VPP quadcopter can be fully controlled around the equilibrium point. This is a significant advantage of VPP quadcopters compared with the conventional ones. The fundamental reason of this advantage is that the VPP control system has eight independent control inputs, whereas a conventional quadcopter only has four. In the future, we will study control of VPP quadcopters subject to two or more propeller failures.

3.4 | Controllability analysis of conventional quadcopters

For comparison purposes, we analyze the controllability of conventional fixed-pitch quadcopters with one motor failure in this section. We consider a specific mechanical configuration where motors located on arms with the same axis spin in opposite directions. For such a configuration, a fixed-pitch quadcopter has an equilibrium when one motor fails.

Suppose propeller 1 of a conventional quadcopter fails to provide any thrust or torque. The dynamical model (1) and input Equation (4) also apply to the conventional quadcopter. The only difference is that the pitch angles α_i in Equation (4) are identical and constant and hence could be merged with the coefficients k_i in Equation (4) to form a new coefficient k_{ci}, where the subscript c denotes "conventional". Note that motor 2 and motor 4 spin in opposite directions such that there exists an equilibrium state when motor 1 fails. As a result, Equation (4) becomes

$$\begin{aligned} u_{c1} &= k_{c1}(\omega_{c2}^2 + \omega_{c3}^2 + \omega_{c4}^2), \\ u_{c2} &= k_{c1}\omega_{c3}^2, \\ u_{c3} &= k_{c1}(\omega_{c4}^2 - \omega_{c2}^2), \\ u_{c4} &= k_{c2}(\omega_{c3}^2 - \omega_{c2}^2 - \omega_{c4}^2) \\ &\quad + k_{c3}(\omega_{c3} - \omega_{c2} - \omega_{c4}), \end{aligned} \tag{17}$$

with k_{c1}, k_{c2}, k_{c3} as constant parameters. As can be seen from Equation (17), ω_{ci} with $i = 2, 3, 4$ are the independent control quantities. Denote $\mathbf{z}_c = [\omega_{c2}, \omega_{c3}, \omega_{c4}]^T$.

Next we need to identify the equilibrium point and linearize the model. Consider the equilibrium state

$$\mathbf{x}_c^* = \left[x_c^*, y_c^*, z_c^*, 0, 0, \psi_c^*, 0, 0, 0, 0, 0, 0\right]^T.$$

It can be calculated that, in order to stay at the equilibrium state, the control quantities should be

$$\begin{aligned} \mathbf{z}_c^* &= \left[\omega_{c2}^*, \omega_{c3}^*, \omega_{c4}^*\right], \\ &= \left[\frac{mg}{2k_{c1}}, 0, \frac{mg}{2k_{c1}}\right]. \end{aligned}$$

Let $\overline{\mathbf{z}}_c = \mathbf{z}_c - \mathbf{z}_c^*$ and $\overline{\mathbf{x}}_c = \mathbf{x}_c - \mathbf{x}_c^*$. The linearized dynamical equation is

$$\dot{\overline{\mathbf{x}}}_c = \mathbf{A}_c\overline{\mathbf{x}}_c + \mathbf{B}_c\overline{\mathbf{z}}_c, \tag{18}$$

where

$$\begin{aligned} \mathbf{A}_c &= \left.\frac{\partial \mathbf{F}_c(\mathbf{x}_c, \mathbf{z}_c)}{\partial \mathbf{x}_c}\right|_{\mathbf{x}_c=\mathbf{x}_c^*, \mathbf{z}_c=\mathbf{z}_c^*} \\ &= \begin{bmatrix} 0_{3\times3} & 0_{3\times3} & 0_{3\times3} & \mathbf{I}_{3\times3} \\ 0_{3\times3} & 0_{3\times3} & \mathbf{I}_{3\times3} & 0_{3\times3} \\ 0_{3\times3} & 0_{3\times3} & 0_{3\times3} & 0_{3\times3} \\ 0_{3\times3} & \mathbf{E}_{c3\times3} & 0_{3\times3} & 0_{3\times3} \end{bmatrix} \in \mathbb{R}^{12\times12}, \end{aligned}$$

$$\mathbf{E}_{c3\times3} = \begin{bmatrix} g\sin\psi_c^* & g\cos\psi_c^* & 0 \\ -g\cos\psi_c^* & g\sin\psi_c^* & 0 \\ 0 & 0 & 0 \end{bmatrix},$$

and

$$
\mathbf{B}_{\mathrm{c}} = \left.\frac{\partial \mathbf{F}_{\mathrm{c}}(\mathbf{x}_{\mathrm{c}}, \mathbf{z}_{\mathrm{c}})}{\partial \mathbf{z}_{\mathrm{c}}}\right|_{\mathbf{x}_{\mathrm{c}}=\mathbf{x}_{\mathrm{c}}^{*}, \mathbf{z}_{\mathrm{c}}=\mathbf{z}_{\mathrm{c}}^{*}}
= \begin{bmatrix}
0 & 0 & 0 \\
0 & 0 & 0 \\
0 & 0 & 0 \\
0 & 0 & 0 \\
0 & 0 & 0 \\
0 & 0 & 0 \\
0 & k_{\mathrm{c}1}\omega_{\mathrm{c}3}^{*}\frac{l}{I_x} & 0 \\
-k_{\mathrm{c}1}\omega_{\mathrm{c}2}^{*}\frac{l}{I_y} & 0 & k_{\mathrm{c}1}\omega_{\mathrm{c}4}^{*}\frac{l}{I_y} \\
r_2 & -r_3 & -r_4 \\
0 & 0 & 0 \\
0 & 0 & 0 \\
\frac{2k_{\mathrm{c}1}}{m}\omega_{\mathrm{c}2}^{*} & \frac{2k_{\mathrm{c}1}}{m}\omega_{\mathrm{c}3}^{*} & \frac{2k_{\mathrm{c}1}}{m}\omega_{\mathrm{c}4}^{*}
\end{bmatrix} \in \mathbb{R}^{12\times 3},
$$

$$
r_i = -2k_{\mathrm{c}2}\omega_{\mathrm{c}i}^{*} + k_{\mathrm{c}3}\frac{l}{I_z},
$$

with $\mathbf{I}_{3\times 3}$ as identity matrix.

Let $k_{\mathrm{c}1}l\omega_{\mathrm{c}3}^{*}/I_x = c_1$, $-k_{\mathrm{c}1}l\omega_{\mathrm{c}2}^{*}/I_y = c_2$, $r_2 = r_4 = c_3$, and $2k_{\mathrm{c}1}\omega_{\mathrm{c}2}^{*}/m = c_4$. Then, the controllability matrix $\mathbf{Q}_{\mathrm{c}}$ is given in equation

$$
\mathbf{Q}_{\mathrm{c}} = [\mathbf{B}_{\mathrm{c}}\ \mathbf{A}_{\mathrm{c}}\mathbf{B}_{\mathrm{c}}\ \mathbf{A}_{\mathrm{c}}^{2}\mathbf{B}_{\mathrm{c}}\ \dots\ \mathbf{A}_{\mathrm{c}}^{11}\mathbf{B}_{\mathrm{c}}]
= \begin{bmatrix}
0 & 0 & 0 & 0 & 0 & 0 & 0 & 0 & 0 & -c_2 g & 0 & c_2 g & \\
0 & 0 & 0 & 0 & 0 & 0 & 0 & 0 & 0 & 0 & 0 & 0 & \\
0 & 0 & 0 & c_4 & 0 & c_4 & 0 & 0 & 0 & 0 & 0 & 0 & \\
0 & 0 & 0 & 0 & 0 & 0 & 0 & 0 & 0 & 0 & 0 & 0 & \\
0 & 0 & 0 & -c_2 & 0 & c_2 & 0 & 0 & 0 & 0 & 0 & 0 & \\
0 & 0 & 0 & c_3 & \frac{k_{\mathrm{c}3}l}{I_z} & -c_3 & 0 & 0 & 0 & 0 & 0 & 0 & \mathbf{0}_{12\times 24} \\
0 & 0 & 0 & 0 & 0 & 0 & 0 & 0 & 0 & 0 & 0 & 0 & \\
-c_2 & 0 & c_2 & 0 & 0 & 0 & 0 & 0 & 0 & 0 & 0 & 0 & \\
c_3 & \frac{k_{\mathrm{c}3}l}{I_z} & -c_3 & 0 & 0 & 0 & 0 & 0 & 0 & 0 & 0 & 0 & \\
0 & 0 & 0 & 0 & 0 & 0 & -c_2 g & 0 & c_2 g & 0 & 0 & 0 & \\
0 & 0 & 0 & 0 & 0 & 0 & 0 & 0 & 0 & 0 & 0 & 0 & \\
c_4 & 0 & c_4 & 0 & 0 & 0 & 0 & 0 & 0 & 0 & 0 & 0 &
\end{bmatrix}. \tag{19}
$$

It can be counted that the rank of controllability matrix is $\mathrm{rank}(\mathbf{Q}_{\mathrm{c}}) = 8$. Since the full row rank of $\mathbf{Q}_{\mathrm{c}}$ is 12, the linearized system is not fully controllable and there are four uncontrollable modes.

Next, we conduct controllability decomposition to identify the uncontrollable states. Define a new state as $\tilde{\mathbf{x}}_{\mathrm{c}} = \mathbf{T}_{\mathrm{c}}^{-1}\overline{\mathbf{x}}_{\mathrm{c}}$, where $\mathbf{T}_{\mathrm{c}}$ is a transformation matrix. It follows from the linearized model in Equation (18) that

$$
\dot{\tilde{\mathbf{x}}}_{\mathrm{c}} = \mathbf{T}_{\mathrm{c}}^{-1}\mathbf{A}_{\mathrm{c}}\mathbf{T}_{\mathrm{c}}\tilde{\mathbf{x}}_{\mathrm{c}} + \mathbf{T}_{\mathrm{c}}^{-1}\mathbf{B}_{\mathrm{c}}\overline{\mathbf{z}}_{\mathrm{c}}. \tag{20}
$$

Following the controllability decomposition procedure,[21] take 10 linearly independent columns of Equation (19) and add four custom columns to make $\mathbf{T}_c$ nonsingular, as in

$$\mathbf{T}_c = \begin{bmatrix} 0 & 0 & 0 & 0 & 0 & 0 & 0 & -c_2 g & 0 & 0 & 0 & 0 \\ 0 & 0 & 0 & 0 & 0 & 0 & 0 & 0 & 1 & 0 & 0 & 0 \\ 0 & 0 & 0 & c_4 & 0 & c_4 & 0 & 0 & 0 & 0 & 0 & 0 \\ 0 & 0 & 0 & 0 & 0 & 0 & 0 & 0 & 0 & 1 & 0 & 0 \\ 0 & 0 & 0 & -c_2 & 0 & c_2 & 0 & 0 & 0 & 0 & 0 & 0 \\ 0 & 0 & 0 & c_3 & \frac{k_{c3} l}{I_z} & -c_3 & 0 & 0 & 0 & 0 & 0 & 0 \\ 0 & 0 & 0 & 0 & 0 & 0 & 0 & 0 & 0 & 0 & 1 & 0 \\ -c_2 & 0 & c_2 & 0 & 0 & 0 & 0 & 0 & 0 & 0 & 0 & 0 \\ c_3 & \frac{k_{c3} l}{I_z} & -c_3 & 0 & 0 & 0 & 0 & 0 & 0 & 0 & 0 & 0 \\ 0 & 0 & 0 & 0 & 0 & 0 & -c_2 g & 0 & 0 & 0 & 0 & 0 \\ 0 & 0 & 0 & 0 & 0 & 0 & 0 & 0 & 0 & 0 & 0 & 1 \\ c_4 & 0 & c_4 & 0 & 0 & 0 & 0 & 0 & 0 & 0 & 0 & 0 \end{bmatrix}. \tag{21}$$

Then, the new state could be partitioned into controllable component $\tilde{\mathbf{x}}_c$ and uncontrollable component $\tilde{\mathbf{x}}_{uc}$, and Equation (20) becomes

$$\left[\begin{array}{c} \tilde{\mathbf{x}}_c \\ \hline \tilde{\mathbf{x}}_{uc} \end{array}\right]' = \left[\begin{array}{c|c} \mathbf{A}_c & \mathbf{A}_{12} \\ \hline \mathbf{0} & \mathbf{A}_{uc} \end{array}\right] \left[\begin{array}{c} \tilde{\mathbf{x}}_c \\ \hline \tilde{\mathbf{x}}_{uc} \end{array}\right] + \left[\begin{array}{c} \mathbf{B}_c \\ \hline \mathbf{0} \end{array}\right] \overline{\mathbf{z}}_c. \tag{22}$$

Substituting Equation (21) into $\tilde{\mathbf{x}}_c = \mathbf{T}_c^{-1}\overline{\mathbf{x}}_c$ yields

$$\tilde{\mathbf{x}}_c = \begin{bmatrix} \frac{x_{12} m}{2c_4} - \frac{x_8}{2c_2} \\ \frac{x_9}{c_5} + \frac{c_3 x_8}{c_2 c_5} \\ \frac{x_8}{2c_2} + \frac{x_{12}}{2c_4} \\ \frac{x_3}{2c_4} - \frac{x_5}{2c_2} \\ \frac{x_6}{c_5} + \frac{c_3 x_5}{c_2 c_5} \\ \frac{x_5}{2c_2} + \frac{x_3}{2c_4} \\ -\frac{x_{10}}{c_2 g} \\ -\frac{x_1}{c_2 g} \\ x_2 \\ x_4 \\ x_7 \\ x_{11} \end{bmatrix}.$$

According to Equation (22), the last four elements of $\tilde{\mathbf{x}}_c$ correspond to uncontrollable modes. Hence x_2, x_4, x_7, and x_{11} are uncontrollable. Here, x_4 and x_7 represent ϕ and p, respectively, and x_2 and x_{11} represent y and v, respectively.

4 | CONTROLLER DESIGN AND SIMULATION VALIDATION

4.1 | Controller design

Unlike conventional quadcopters, a VPP quadcopter remains controllable in the presence of one propeller failure. Therefore, simple LQR controllers can be designed based on the linearized model derived in preceding sections. This is an advantage of VPP quadcopters compared with the conventional ones.

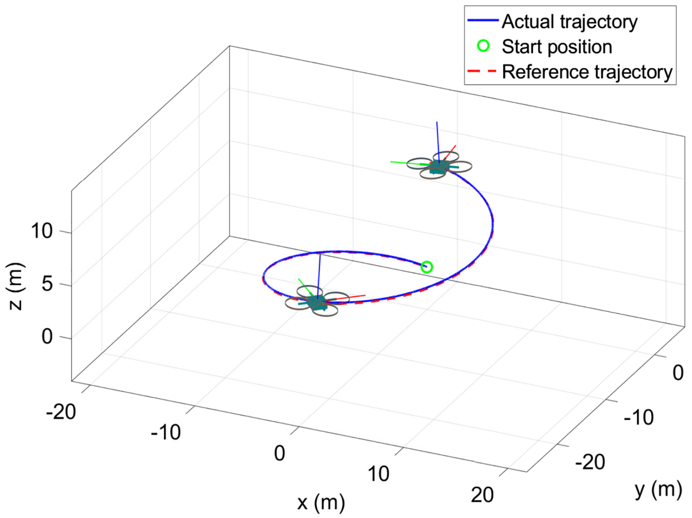

FIGURE 2 Three-dimensional trajectory in scenario 1

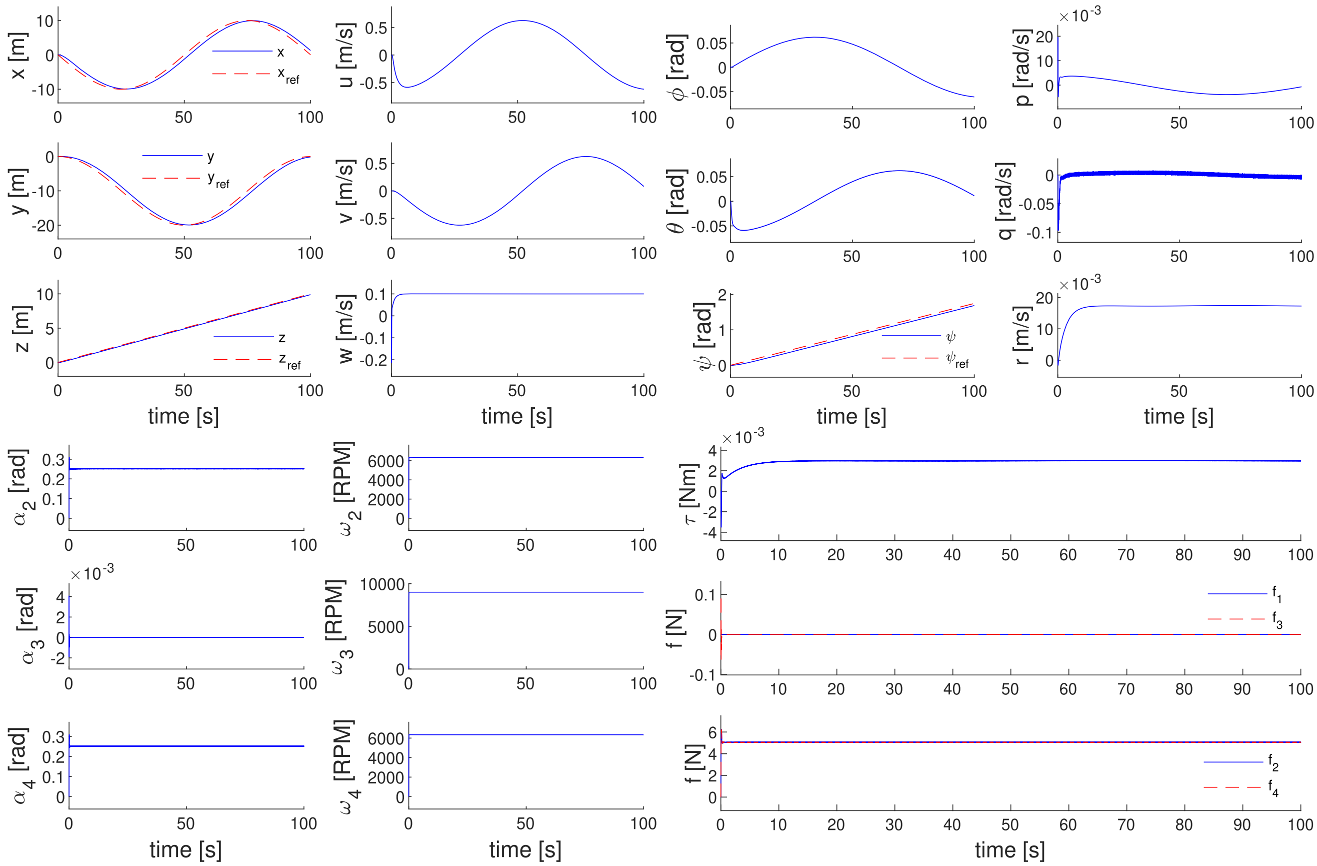

FIGURE 3 Simulation results for scenario 1

4.2 | Simulation examples

We next present three simulation examples to verify the effectiveness of the proposed results. In the simulation, suppose propeller 1 fails to work and hence it gives zero thrust force and zero torque. In the simulation, we model the actuator and speed control of a VPP as a first-order transfer function to approximate their dynamics. The cutoff frequency is chosen as 10 Hz.

FIGURE 4 Three-dimensional trajectory in scenario 2

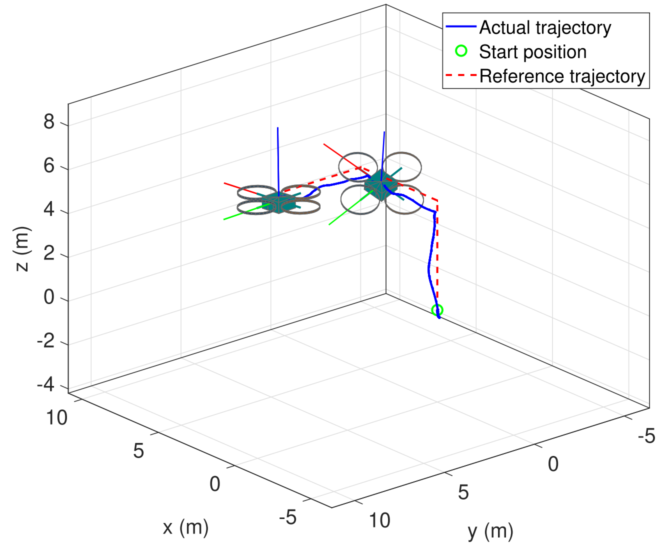

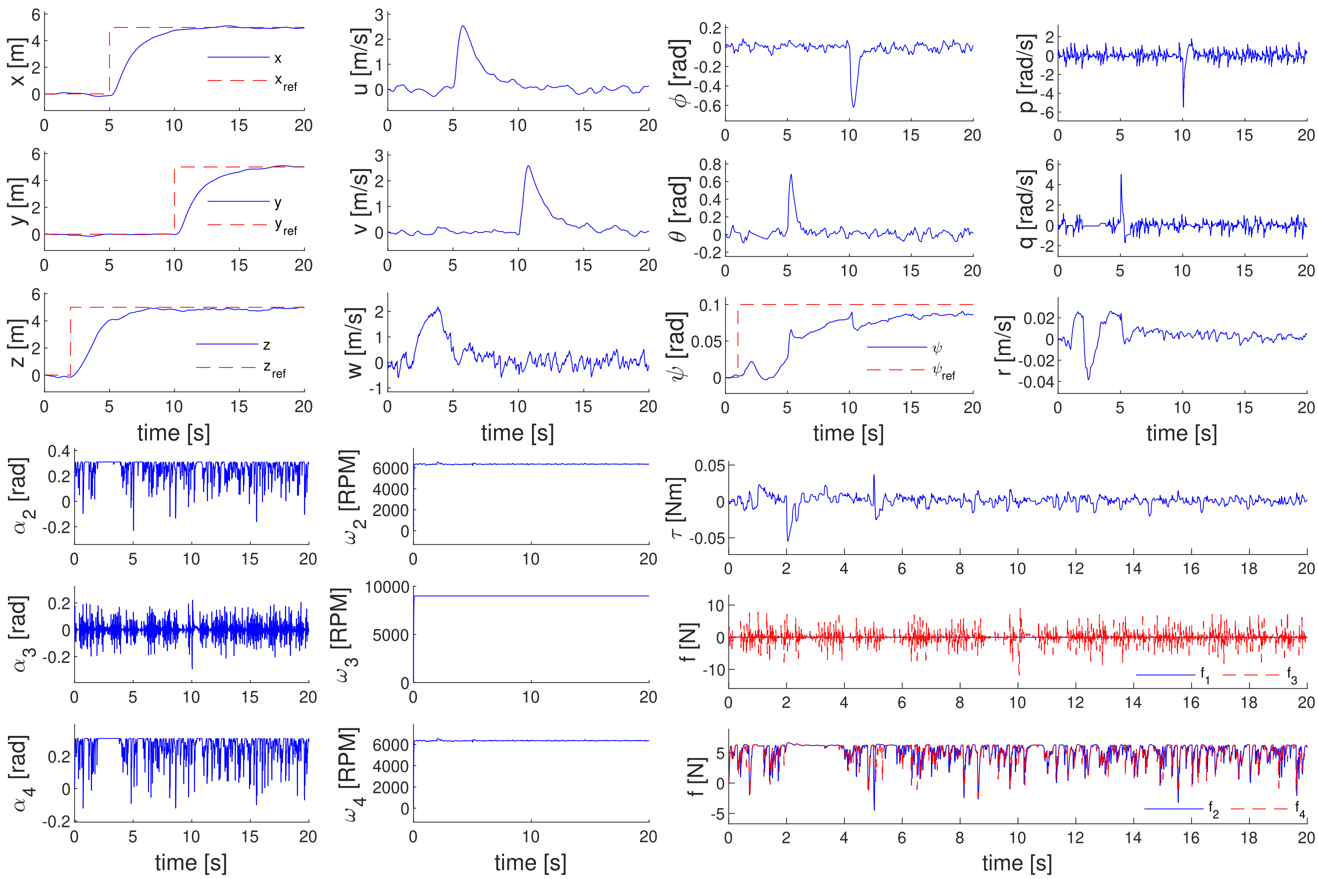

FIGURE 5 Simulation results for scenario 2

4.2.1 | Scenario 1: No noise nor disturbance

In this scenario, we assume that all the states can be measured perfectly and there are no external disturbances. The reference trajectory is a continuous circle combined with increasing altitude and varying orientation.

Simulation results are shown in Figures 2 and 3. As can be seen, the quadcopter remains fully controllable though one propeller fails. Here, the reference tracking is achieved by tracking a moving target point with desired position and altitude.

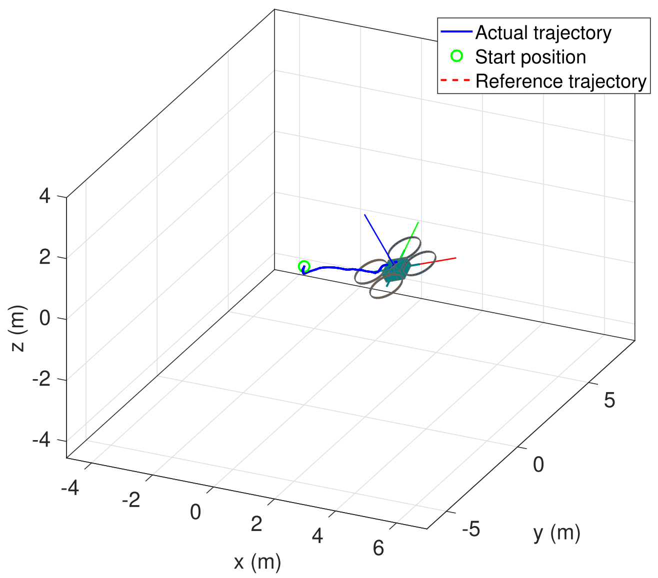

FIGURE 6 Three-dimensional trajectory in scenario 3

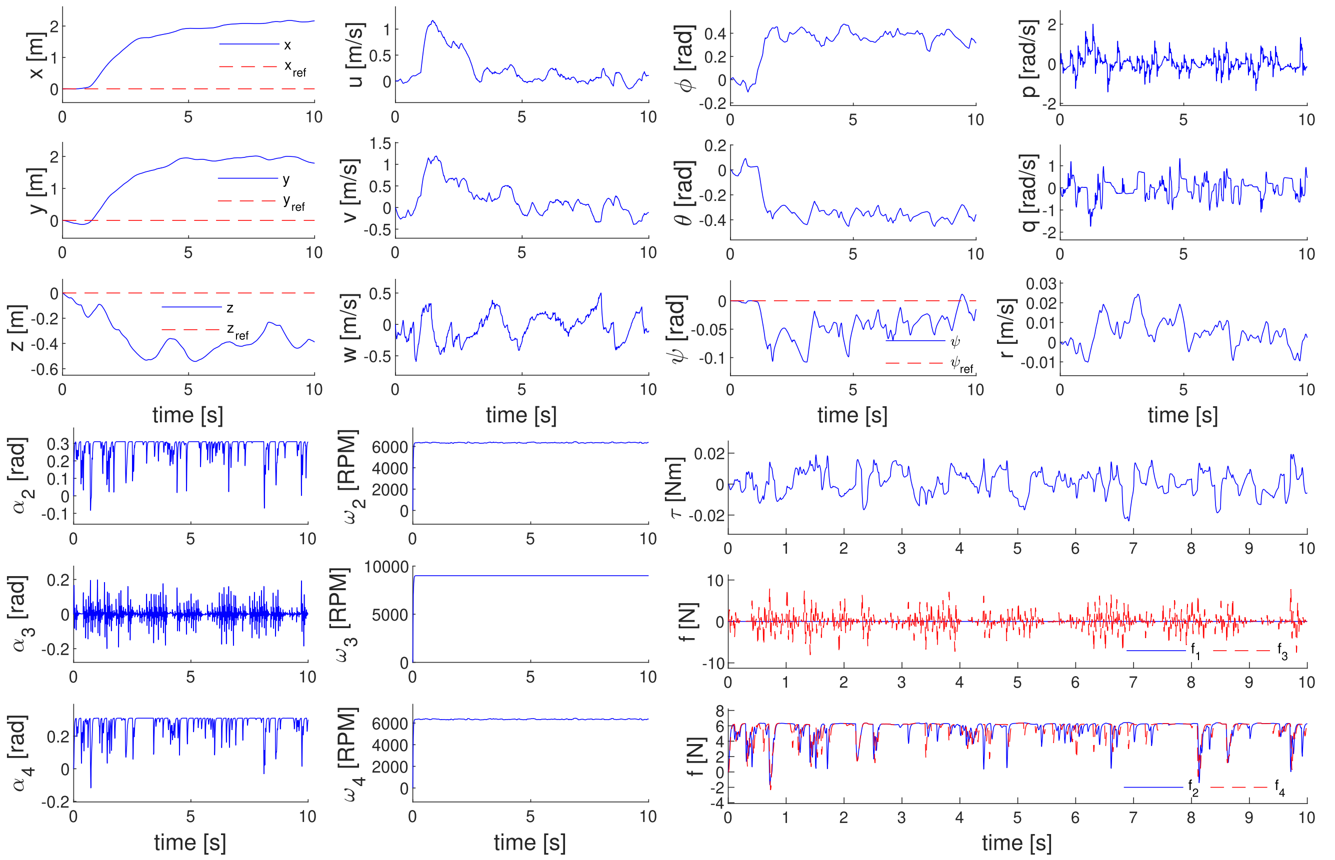

FIGURE 7 Simulation results for scenario 3

4.2.2 | Scenario 2: Measurements with noise

In scenario 2, the quadcopter needs to track the target points varying from [0, 0, 0], [0, 0, 5], [5, 0, 5], and finally to [5, 5, 5] at time $t = 0, 2, 5, 10$, respectively. The desired yaw angle changes from zero to 0.1 rad at $t = 1$. During the whole process, noise with the signal-to-noise ratio as 15 dB is added to all the feedback states.

Figures 4 and 5 show the tracking performance of the VPP quadcopter. The quadcopter can quickly track the reference in the presence of noise.

4.2.3 | Scenario 3: Noise and external disturbance

In scenario 3, we assume that all the state measurements are corrupted by 15 dB signal-to-noise-ratio noise. More importantly, wind disturbance is considered. In particular, the wind disturbance is 4 m/s along x-axis and 4 m/s along y-axis when $t \geq 1$. The desired states are all set to 0. Figure 6 presents the reaction of a VPP quadcopter facing an external disturbance and measurement noise. As can be seen in Figure 7, the pitch and roll angles of the quadcopter converge to constant nonzero values to counter the wind disturbance.

5 | CONCLUSIONS

This article studied the control of a VPP quadcopter in the presence of a propeller failure. It has been shown that the VPP quadcopter remains fully controllable and a simple LQR controller has been designed. Although the controllability analysis and controller design are both based on the linearized model, numerical simulation incorporating external disturbances, and measurement noise has verified that the theoretical findings are still valid for the nonlinear dynamical model. It is suggested that VPP quadcopters provide a promising platform for various aerial tasks. The proposed controller could be extended to stabilize the quadcopter when the fault occurs during the normal flight in the future. In addition, we will study other fault-tolerant problems such as failure detection, isolation, and switching control of VPP quadcopters.

ORCID

Shiyu Zhao https://orcid.org/0000-0003-3098-8059

REFERENCES

1. Van M. An enhanced robust fault tolerant control based on an adaptive fuzzy pid-nonsingular fast terminal sliding mode control for uncertain nonlinear systems. IEEE/ASME Trans Mech. 2018;23(3):1362-1371.
2. Liu Z, Yuan C, Zhang Y, Luo J. A learning-based fault tolerant tracking control of an unmanned quadrotor helicopter. J Intell Robot Syst. 2016;84(1-4):145-162.
3. Sharifi F, Mirzaei M, Gordon BW, Zhang Y. Fault tolerant control of a quadrotor UAV using sliding mode control. Paper presented at: Proceedings of the 2010 Conference on Control and Fault-Tolerant Systems; 2010:239-244.
4. Zhang Y, Jiang J. Bibliographical review on reconfigurable fault-tolerant control systems. Annu Rev Control. 2008;32(2):229-252.
5. Chen F, Jiang R, Zhang K, Jiang B, Tao G. Robust backstepping sliding-mode control and observer-based fault estimation for a quadrotor UAV. IEEE Trans Ind Electron. 2016;63(8):5044-5056.
6. Zhong Y, Liu Z, Zhang Y, Zhang W, Zuo J. Active fault-tolerant tracking control of a quadrotor with model uncertainties and actuator faults. Front Inf Technol Electron Eng. 2019;20(1):95-106.
7. Chamseddine A, Theilliol D, Zhang Y, Join C, Rabbath CA. Active fault-tolerant control system design with trajectory re-planning against actuator faults and saturation: application to a quadrotor unmanned aerial vehicle. Int J Adapt Control Signal Process. 2015;29(1):1-23.
8. Cutler M, Ure NK, Michini B, How J. Comparison of fixed and variable pitch actuators for agile quadrotors. Paper presented at: Proceedings of the AIAA Guidance, Navigation, and Control Conference; 2011:6406-6423.
9. Cutler M, How J. Actuator constrained trajectory generation and control for variable-pitch quadrotors. Paper presented at: Proceedings of AIAA Guidance, Navigation, and Control Conference; 2012:4777-4792.
10. Cutler M, How JP. Analysis and control of a variable-pitch quadrotor for agile flight. J Dyn Syst Meas Control. 2015;137(10):101002-101016.
11. Gupta N, Kothari M. Flight dynamics and nonlinear control design for variable-pitch quadrotors. Paper presented at: Proceedings of 2016 American Control Conference (ACC)IEEE; 2016:3150-3155.
12. Sheng S, Sun C. Control and optimization of a variable-pitch quadrotor with minimum power consumption. Energies. 2016;9(4):232-250.
13. Mueller MW, D'Andrea R. Stability and control of a quadrocopter despite the complete loss of one, two, or three propellers. Paper presented at: Proceedings of the 2014 IEEE International Conference on Robotics and Automation; 2014:45-52.
14. Qi X, Qi J, Theilliol D, Song D, Zhang Y, Han J. Self-healing control design under actuator fault occurrence on single-rotor unmanned helicopters. J Intell Robot Syst. 2016;84(1-4):21-35.
15. Freddi A, Lanzon A, Longhi S. A feedback linearization approach to fault tolerance in quadrotor vehicles. IFAC Proc Vol. 2011;44(1):5413-5418.
16. Mueller MW, D'Andrea R. Relaxed hover solutions for multicopters: application to algorithmic redundancy and novel vehicles. Int J Robot Res. 2016;35(8):873-889.
17. Merheb AR, Noura H, Bateman F. Emergency control of AR drone quadrotor UAV suffering a total loss of one rotor. IEEE/ASME Trans Mech. 2017;22(2):961-971.
18. Bristeau P, Martin P, Salaün E, Petit N. The role of propeller aerodynamics in the model of a quadrotor UAV. Paper presented at: Proceedings of 2009 European Control Conference; 2009:683-688.

19. Powers C, Mellinger D, Kushleyev A, Kothmann B, Kumar V. Influence of aerodynamics and proximity effects in quadrotor flight. In: Desai JP, Dudek G, Khatib O, Kumar V, eds. Springer Tracts in Advanced Robotics. Vol 88. Heidelberg, Germany: Springer; 2013:289-302.
20. Ent CY. Stingray 500; 2016. Accessed: September 1, 2019.
21. Boley D. Computing the Kalman decomposition: an optimal method. IEEE Trans Autom Control. 1984;29(1):51-53.

How to cite this article: Wang Z, Groß R, Zhao S. Controllability analysis and controller design for variable-pitch propeller quadcopters with one propeller failure. *Adv Control Appl*. 2020;2:e29. https://doi.org/10.1002/adc2.29